

## Nonlinear seismic damage control of steel frame-steel plate shear wall structures using MR dampers

Longhe Xu<sup>\*1</sup>, Zhongxian Li<sup>2</sup> and Yang Lv<sup>2</sup>

<sup>1</sup>School of Civil Engineering, Beijing Jiaotong University, Beijing 100044, China

<sup>2</sup>School of Civil Engineering, Tianjin University, Tianjin 300072, China

(Received April 20, 2014, Revised May 6, 2014, Accepted May 7, 2014)

**Abstract.** A semi-active control platform comprising the mechanical model of magnetorheological (MR) dampers, the bang-bang control law and damage material models is developed, and the simulation method of steel plate shear wall (SPSW) and optimization method for capacity design of MR dampers are proposed. A 15-story steel frame-SPSW structure is analyzed to evaluate the seismic performance of nonlinear semi-active controlled structures with optimal designed MR dampers, results indicate that the control platform and simulation method are stable and fast, and the damage accumulation effects of uncontrolled structure are largely reduced, and the seismic performance of controlled structures has been improved.

**Keywords:** steel plate shear wall; magnetorheological (MR) damper; control platform; nonlinear analysis; seismic damage control;

---

### 1. Introduction

Controlling the damage process and failure mode, avoiding the global collapse, and increasing the seismic safety of structures are of great significance to the casualties' reduction and seismic losses mitigation. Structural control has been proved to be an effective technique to improve the seismic resistance of structures through energy dissipation by supplemental devices. During the last several decades, semi-active control methods have been widely studied due to the effectiveness, robustness and minimum operating requirements. Magnetorheological (MR) dampers are typical semi-active devices and have lots of attractive characteristics for use in structural vibration suppression, and several models have been developed for portraying the dynamic behavior of MR dampers, such as neural network-based models (Wang and Liao 2005), fuzzy logic-based models (Kim *et al.* 2008), the Bingham model (Lee and Wereley 2000), and the most popularly used Bouc-Wen hysteresis model (Jansen and Dyke 2000).

A variety of semi-active control algorithms have been developed and proved to be effective and stable, such as decentralized bang-bang control (Feng and Shinozuka 1990), modified linear quadratic regulator (Johnson and Erkus 2007), clipped-optimal control (Dyke and Spencer 1996), multi-step predictive control (Xu and Li 2008, 2011), and trust-region based instantaneous optimal

---

\*Corresponding author, Professor, Email: [lhxu@bjtu.edu.cn](mailto:lhxu@bjtu.edu.cn)

semi-active control (Lin *et al.* 2008). These control algorithms are based on active control algorithms which the optimal active control force should be calculated firstly, and semi-active control laws are used to determine the command voltages of MR dampers to allow the damping force approaching to the target. Most of the algorithms are suitable to the linear structural control under small or medium earthquake motions, to consider the nonlinear properties of practical structures, the third generation (Ohtori *et al.* 2004) of benchmark model was proposed and has made some achievements (Yoshida and Dyke 2004, Wongprasert and Symans 2004) in the field of nonlinear semi-active control strategy. Because of the strong uncertainty of the potential earthquakes in future, even the controlled structure using MR dampers may experience damage and collapse as well. In addition, the simplification of the finite element model of control systems seems impossible to precisely predict the nonlinear responses of the practical structure.

In this paper, the semi-active control platform comprising the Bouc-Wen model of MR dampers, the simple bang-bang semi-active control law and the steel damage material model is developed, the simulation method of SPSW, the damage criteria of steel frame and the optimal designed control force of MR dampers are proposed. Based on the data transferring between the main program and the subroutines, a 15-story steel frame-SPSW structure is analyzed and compared to verify the nonlinear seismic control effectiveness on the control platform.

## 2. Nonlinear control formulation

### 2.1. Control equation

The performance of the practical structures will degenerate during their service time, so all the structures are time-varying nonlinear systems. Considering the  $n$  degree of freedoms structure with  $r$  control devices, the basic control equation under excitations is,

$$\mathbf{M}\ddot{\mathbf{X}}(t) + \mathbf{C}\dot{\mathbf{X}}(t) + \mathbf{K}\mathbf{X}(t) = \mathbf{E}_s\mathbf{P}(t) + \mathbf{B}_s\mathbf{U}(t) \quad (1)$$

where  $\mathbf{M}$ ,  $\mathbf{C}$  and  $\mathbf{K}$  are  $n \times n$  mass, damping and stiffness matrices, respectively;  $\mathbf{X}$ ,  $\dot{\mathbf{X}}$  and  $\ddot{\mathbf{X}}$  are  $n$ -dimensional displacement, velocity and acceleration vectors, respectively;  $\mathbf{P}(t)$  and  $\mathbf{U}(t)$  are excitation and control force vectors, respectively;  $\mathbf{E}_s$  and  $\mathbf{B}_s$  are  $n \times n$  and  $n \times r$  location matrices of excitations and control forces, respectively. The control equation can be divided into the controlled degrees of freedom and normal degrees of freedom and rewritten in the partitioned form as follows,

$$\begin{bmatrix} \mathbf{M}_c & \mathbf{M}_{cn} \\ \mathbf{M}_{nc} & \mathbf{M}_n \end{bmatrix} \begin{Bmatrix} \ddot{\mathbf{X}}_c(t) \\ \ddot{\mathbf{X}}_n(t) \end{Bmatrix} + \begin{bmatrix} \mathbf{C}_c & \mathbf{C}_{cn} \\ \mathbf{C}_{nc} & \mathbf{C}_n \end{bmatrix} \begin{Bmatrix} \dot{\mathbf{X}}_c(t) \\ \dot{\mathbf{X}}_n(t) \end{Bmatrix} + \begin{bmatrix} \mathbf{K}_c & \mathbf{K}_{cn} \\ \mathbf{K}_{nc} & \mathbf{K}_n \end{bmatrix} \begin{Bmatrix} \mathbf{X}_c(t) \\ \mathbf{X}_n(t) \end{Bmatrix} = \begin{Bmatrix} \mathbf{P}_c(t) + \mathbf{U}(t) \\ \mathbf{P}_n(t) \end{Bmatrix} \quad (2)$$

where, the subscript c and n represent the controlled and normal degree of freedoms, respectively;  $\mathbf{M}_c$ ,  $\mathbf{C}_c$  and  $\mathbf{K}_c$  are  $r \times r$  controlled mass, damping and stiffness matrices, respectively;  $\mathbf{M}_n$ ,  $\mathbf{C}_n$  and  $\mathbf{K}_n$  are  $(n-r) \times (n-r)$  uncontrolled mass, damping and stiffness matrices, respectively;  $\mathbf{M}_{cn}$  ( $\mathbf{M}_{nc}$ ),  $\mathbf{C}_{cn}$  ( $\mathbf{C}_{nc}$ ) and  $\mathbf{K}_{cn}$  ( $\mathbf{K}_{nc}$ ) are the coupling mass, damping and stiffness matrices respectively; and the displacements, velocities and accelerations are partitioned into two vectors according to the

control device locations. In LS-DYNA program, all the elements of the coupling matrixes are 0, so the control equation can be rewritten into  $r$  controlled equations and  $n-r$  normal equations of single degree of freedom,

$$m_c \ddot{x}_c(t) + c_c \dot{x}_c(t) + k_c x_c(t) = p_c(t) + u(t) \tag{3}$$

$$m_n \ddot{x}_n(t) + c_n \dot{x}_n(t) + k_n x_n(t) = p_n(t) \tag{4}$$

In the control platform, the control device is simulated by a virtual beam element and is embedded into the global finite element model of the structure, so the direction and intensity of the control force is adaptive with the structural deformation. In Eq. (3),  $u(t)$  is the control force getting from the subroutines of semi-active controller and MR damper model. Using the central difference method and omitting the subscript of variables, the expressions for velocity and acceleration at time  $t$  are as follows,

$$\dot{x}(t) = \frac{x(t + \Delta t) - x(t - \Delta t)}{2\Delta t} \tag{5}$$

$$\ddot{x}(t) = \frac{x(t + \Delta t) - 2x(t) + x(t - \Delta t)}{(\Delta t)^2} \tag{6}$$

Substituting these approximate expressions into the control Eq. (3), and assuming that the system is linearly elastic over the duration  $\Delta t$ , that is,

$$m \frac{x(t + \Delta t) - 2x(t) + x(t - \Delta t)}{(\Delta t)^2} + c \frac{x(t + \Delta t) - x(t - \Delta t)}{2\Delta t} + kx(t) = p(t) + u(t) \tag{7}$$

Variables at time  $t$  and  $t-\Delta t$  in Eq. (7) are assumed known, transferring these known quantities to the right side of equation, that is,

$$\left[ \frac{m}{(\Delta t)^2} + \frac{c}{2\Delta t} \right] x(t + \Delta t) = p(t) + u(t) - \left[ \frac{m}{(\Delta t)^2} - \frac{c}{2\Delta t} \right] x(t - \Delta t) - \left[ k - \frac{2m}{(\Delta t)^2} \right] x(t) \tag{8}$$

or,

$$\hat{k}x(t + \Delta t) = \hat{p}(t) \tag{9}$$

where  $\hat{k}$  and  $\hat{p}(t)$  are respectively given by,

$$\hat{k} = \frac{m}{(\Delta t)^2} + \frac{c}{2\Delta t} \tag{10}$$

And

$$\hat{p}(t) = p(t) + u(t) - \left[ \frac{m}{(\Delta t)^2} - \frac{c}{2\Delta t} \right] x(t - \Delta t) - \left[ k - \frac{2m}{(\Delta t)^2} \right] x(t) \tag{11}$$

Variable  $x(t+\Delta t)$  can be determined from the equilibrium condition as,

$$x(t + \Delta t) = \frac{\hat{p}(t)}{\hat{k}} \tag{12}$$

For the uncontrolled degree of freedoms, the main program solves it using the same method except for calling the control platform.

### 2.2 Control platform

To implement the semi-active control strategy in general finite element software, the transducers, the semi-active controller and the actuators should be developed into the subroutines, and unobstructed contact with the main program besides has the advantages of fast computation, numerical stable and high precise.

The control platform is shown in Fig. 1, a simple Bouc-Wen model (Jansen and Dyke 2000) is used to portray the behavior of MR damper, and the parameters of this model are scaled up to have maximum capacity of 1000 kN and same with that of Yoshida, *ea al.* (2004). Firstly, the finite element model of structure is built through the pre-processor of the main program, and the material models, element types, contact definition, boundary and loading conditions are all reasonably defined, then the structural dynamic responses at time  $t$  are calculated, together with the state of MR dampers are gathered by the transducers, which are transported to the subroutine of semi-active controller to calculate the required voltages of each MR damper, and the command voltages are applied to the subroutine of Bouc-Wen model to calculate the control forces exerted on the structure, and the structural responses at time  $t+\Delta t$  are calculated. The control process is conducted step by step, and finally, the results are analyzed and evaluated through the post-processor of the main program.

Both the main program and the subroutines of LS-DYNA software are based on explicit integration method which the mass and stiffness matrices are uncoupled, therefore, the active control strategy based semi-active control method is unsuitable for this control platform. What's more, the practical structures experience degenerated performance during strong earthquakes, and the controller designed by the initial stiffness matrix may lead the control process unstable and divergent, so the simple bang-bang control law is employed in this platform as follows,

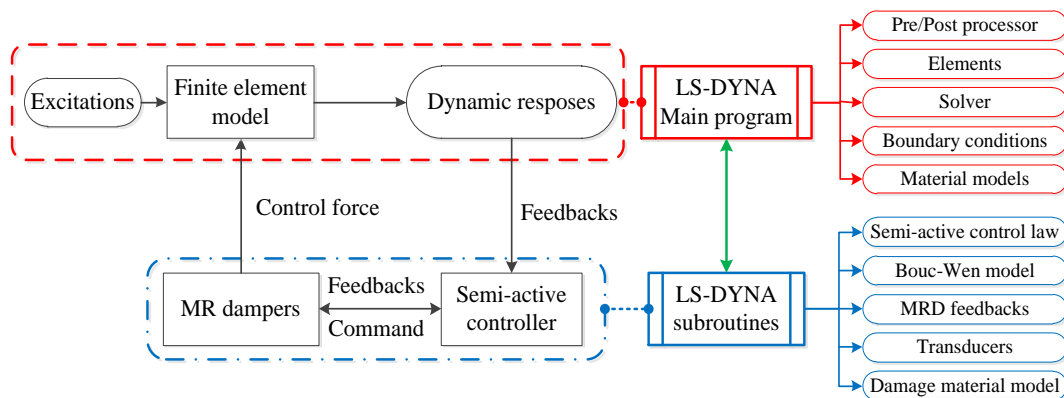


Fig. 1 The frame of semi-active control platform in LS-DYNA program

$$F(t) = \begin{cases} F_{I,\max} & x\dot{x} > 0 \\ F_{I,\min} & x\dot{x} \leq 0 \end{cases} \quad (13)$$

where  $F(t)$  is the control force produced by MR damper at time  $t$ ;  $F_{I,\max}$  and  $F_{I,\min}$  are the maximum and minimum control forces that MR dampers can produce at this moment.

### 3. Damage criteria

The global damage index of structure can be defined as the weighted average value of the local damage indices or the change of modal parameters, while the latter one cannot simulate the locations and damage process of structure. The damage index of the  $j$ th floor of structure is defined as,

$$D_j = \frac{\sum_i \xi_{ij} d_{ij}}{\sum_i \xi_{ij}} \quad (14)$$

where  $\xi_{ij}$  and  $d_{ij}$  are the importance coefficient and the damage index of the  $i$ th category member at the  $j$ th story, and the classification of structural components is based on the boundary condition, member dimension and material properties.

Because of the series connection of each story, the global damage index of structure is defined as the maximum damage index of stories,

$$D_g = \max\{D_j\} \quad (15)$$

The existence of damage will cause the modification of structural vibration modes (Salawu 1997), which are manifested as changes in the modal parameters, especially the natural frequencies, which are significantly depended on the location and severity of damage. On the contrary, if a constant damage is assigned artificially to the evaluated structural member one by one, the changes of the modal parameters can reflect the importance of different members contributing to the seismic capacity of the system. Here, it is assumed that one of the  $i$ th kinds of members at the  $j$ th floor is totally damaged and make a stiffness reduction of  $\Delta\mathbf{K}$  and unchanged mass matrix, so the frequencies of the original structure and damage assigned structure can be solved by the characteristic equation.

The importance coefficient of the  $i$ th component at the  $j$ th floor is defined as,

$$\xi_{ij} = \sum_k \frac{\Delta f_{ij,k}}{f_k} \quad (16)$$

where  $\Delta f_{ij,k}$  is the change of the  $k$ th frequency when one of the  $i$ th category of structural members at the  $j$ th story has been eliminated, and  $f_k$  is the  $k$ th frequency of the original structure without damage.

The damage index of beam element is averaged through all the sections of the fiber beam element as depicted in Fig. 2, and the damage index of the  $i$ th column at the  $j$ th floor of structure is given by,

$$d_{ij} = \max\{d_{ij}^e\} \quad (17)$$

where  $d_{ij}^e$  is the averaged damage value of the sections in the  $e$ th element of the member, and the damage index of each fiber is calculated through the Bonora (1997) damage material model using fiber beam element approach. The plastic potential  $f_p$  of the material model is defined as,

$$f_p = \sigma_{eq} - k(\kappa) - \frac{3}{4\alpha_\infty} \alpha'_{ij} \alpha'_{ij} - \sigma_y \quad (18)$$

where  $\sigma_y$  is the initial uniaxial yield stress,  $\alpha_\infty$  is kinematic hardening saturation value;  $\sigma_{eq}$  is the equivalent stress and is calculated by,

$$\sigma_{eq} = \left[ \frac{3}{2} \left( \frac{s_{ij}}{1-d} - \alpha'_{ij} \right) \left( \frac{s_{ij}}{1-d} - \alpha'_{ij} \right) \right]^{1/2} \quad (19)$$

where  $s_{ij}$  and  $\alpha'_{ij}$  are the deviatoric component of stress and kinematic hardening tensor, respectively.  $k$  is the isotropic hardening stress, and is defined through Osgood equation,

$$k(\kappa) = \frac{E_h}{\beta} [1 - \exp(-\beta\kappa)] \quad (20)$$

where  $E_h$  is the isotropic hardening modulus,  $\beta$  is isotropic hardening parameter, which set  $\beta=0$  for linear isotropic hardening,  $\kappa$  is the isotropic hardening coefficient and is defined as the equivalent accumulated plastic strain,

$$\kappa = \varepsilon_p = \int d\varepsilon_p \quad (21)$$

The plastic strain components and the internal variables associated to  $k$  and  $\alpha'_{ij}$  can be derived from  $f_p$  by the normality rule,

$$d\varepsilon_{ij}^p = d\lambda \frac{\partial f_p}{\partial \sigma_{ij}} = \frac{3}{2} \frac{d\lambda}{1-d} \frac{\frac{s_{ij}}{1-d} - \alpha'_{ij}}{\sigma_{eq}} \quad (22)$$

$$d\alpha'_{ij} = C(1-d)d\varepsilon_{ij}^p - \frac{3C}{2\alpha_\infty} \alpha'_{ij} d\lambda \quad (23)$$

$$d\kappa = -d\lambda \frac{\partial f_p}{\partial k} = d\lambda = (1-d)d\varepsilon_p \quad (24)$$

where  $C$  is the kinematic hardening modulus, and  $\lambda$  is the plastic multiplier,

$$d\varepsilon_p = \left(\frac{2}{3} d\varepsilon_{ij}^p d\varepsilon_{ij}^p\right)^{1/2} \tag{25}$$

The damage dissipation potential (Bonora 1997) is expressed as,

$$f_d = \left[\frac{1}{2} \left(-\frac{Y}{S_0}\right)^2 \frac{S_0}{1-d}\right] \frac{(d_{cr} - d)^{1-1/\nu}}{\kappa^{(2+n)/n}} \tag{26}$$

The kinetic law of damage evolution is given by,

$$\dot{d} = -d\lambda \frac{\partial f_d}{\partial Y} = \frac{(d_{cr} - d_0)^{1/\nu}}{\ln(\varepsilon_u - \varepsilon_{th})} f\left(\frac{\sigma_m}{\sigma_{eq}}\right) (d_{cr} - d)^{1-1/\nu} \frac{d\kappa}{\kappa} \tag{27}$$

where  $Y$  is the variable associated to damage,  $\nu$  and  $S_0$  are material parameters,  $\varepsilon_u$  and  $\varepsilon_{th}$  are the critical and threshold equivalent accumulated plastic strain,  $d_{cr}$  and  $d_0$  are critical and initial damage of the material corresponding to  $\varepsilon_u$  and  $\varepsilon_{th}$ , respectively.

The damage plastic steel model is applied to fiber beam element model, and a typical hysteretic curve and corresponding damage evolution under fully reversed cycling are shown in Fig. 3 and 4, respectively, the element failed after about 6 reversals at 20% cyclic strain (Pirondi *et al.* 2006), and the material parameters are listed in Table 1.

Table 1 Material parameters

Parameters	Damage parameters				Plastic parameters				
	$\varepsilon_{th}$	$\varepsilon_{cr}$	$d_{cr}$	$d_0$	$\alpha$	$E_h(\text{MPa})$	$\alpha_{sc}(\text{MPa})$	$C(\text{MPa})$	$\beta$
Value	0.001	0.24	0.065	0	0.2173	200	300	800	0.5

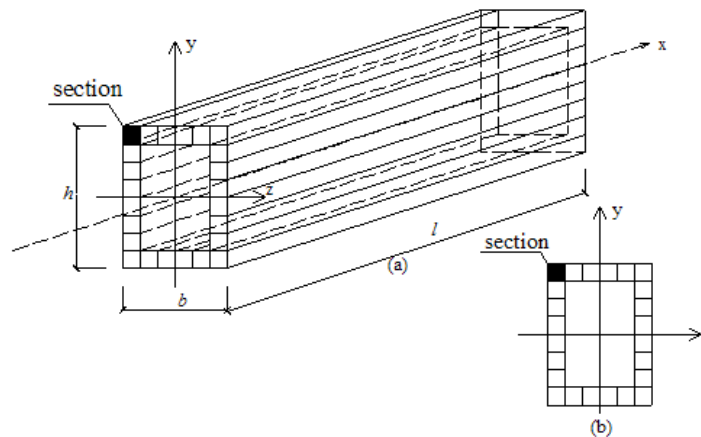


Fig. 2 The discretization of structural member

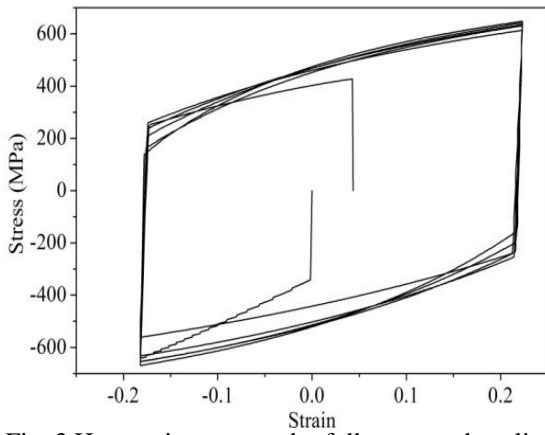


Fig. 3 Hysteretic curve under fully reversed cycling

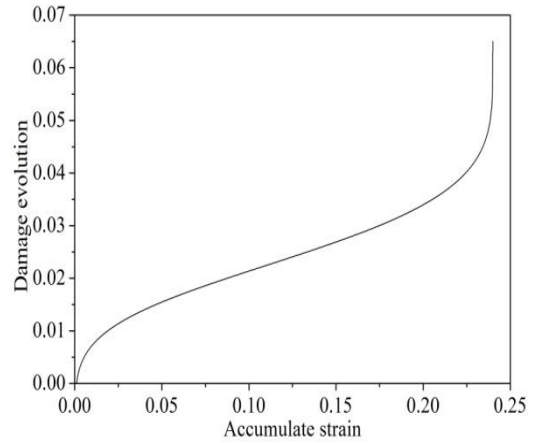


Fig. 4 Damage evolution

#### 4. Control force optimization

In the control systems, MR dampers provide additional energy dissipation capacity while causing slight disturbance to the stiffness of the original structure, the optimization design of MR dampers should consider both the capacity of devices and the demand of original structure. Li *et al.* (2010) proposed a two-phase optimization process using genetic algorithms for optimal placement of MR dampers for the nonlinear benchmark structure, and simulation results indicate that the lower and upper stories will be the first choice for the location of dampers. Liu *et al.* (1997), Li *et al.* (2002) and Lu *et al.* (2003) also investigated the optimal design of MR dampers. However, the optimization methods are not feasible when structures experience strong nonlinear responses. Considering the demand of the main structure and the capacity of supplemental devices, an index combined with the importance coefficient, damage index and internal energy is proposed in this paper to optimize the output force capacity of MR dampers at each story, and the capacity of MR damper at the  $j$ th story is defined as,

$$F_j = \max\{F_j^{mn}\} \quad (m=1, 2, \dots, M; n=1, 2, \dots, N) \quad (28)$$

$$F_{mn}^j = \frac{IC_j DI_j^{mn} E_j^{mn}}{IC_r DI_r^{mn} E_r^{mn}} F_r \quad (29)$$

where  $n$  and  $m$  are the  $n$ th performance levels of the  $m$ th earthquake motion,  $DI_r^{mn}$  is the damage index of the reference story of structure,  $F_r$  is the control force of the reference story, which is determined by the requirement of structure and the capacity of MR dampers.  $E_j^{mn}$  and  $E_r^{mn}$  are the internal energy of the  $j$ th story and the reference story during the  $n$ th performance level of the  $m$ th earthquake motion, respectively.  $IC_j$  and  $IC_r$  are the importance coefficient of the  $j$ th story and the reference story.

### 5. Numerical examples

#### 5.1 Simulation of steel frame-SPSW structures

The analysis models (Foutch and Yun 2002) for steel column, beam and floor slab can be classified as linear or nonlinear centerline models with or without panel zones. The linear model is not suitable for forecasting the distribution of inelastic characteristics and damage properties, and the nonlinear centerline model will underestimate the contribution of floor slab to the stiffness of frame beams. Here, the steel frame is simulated by the fiber element model employing a Hughes-Liu formulation, and the non-coincidence of neutral axis between the frame beam and the floor slab is simulated by translating the slab bottom to the top flange of the steel beam, as shown in Fig. 5(c), each structural member is discretized into a number of sections, and each section is further divided into a number of fibers, as shown in Fig. 5 (b). The sections are located either at the center of the element or at its Gaussian integration points, that the behavior of each fiber can be tracked using a simple uniaxial material model allowing an easy and efficient implementation of the inelastic behavior, and finite transverse shear strains of Hughes-Liu element formulation is also retained comparing to the general fiber beam element, which gives a more reasonable simulation results when shear effects are significant in the squat column.

A conventional SPSW comprises thin unstiffened steel plates and bounded components of steel columns and beams as shown in Fig. 5 (a). There are three strategies to simulate the SPSW, i.e. the shell element method which both the boundary components and the steel plates are simulated by the shell elements, the mixture method which the boundary steel members are simulated by fiber beam elements while the steel plates are simulated by shell elements, and the strip method (Thorburn *et al.* 1983). The strip method has high accurate in simulating the hysteresis of SPSWs in plane force, but it cannot simulate the outside plane moment, the combination of shear and axial force, and the forces interaction at the intersection of shear walls. In this paper, the mixture method is used to simulate the SPSWs, as shown in Fig. 5(d), the steel plate is divided into several layers, and the strain and curvature of the neutral layer are firstly calculated, based on the plane-section assumption of strain and the curvature of the other layers are decided, and the element

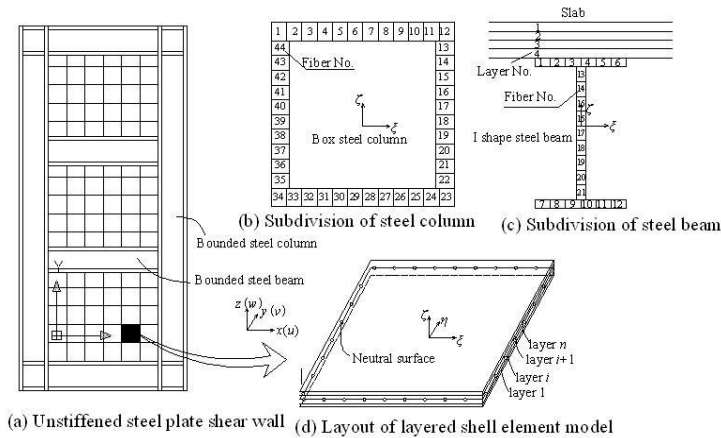


Fig. 5 Schematic diagram of analytical finite element model of SPSW

internal force is integrated through the element thickness corresponding to the material models of each layer. For the layered shell element in LS-DYNA program, the shear strain can also be simulated, and based on the central difference method the numerical converge problem is avoided.

## 5.2 Structural parameters

The analysis structure is 22.2×22.8 m in plan and 15 stories with 3.9 m high each in elevation and its typical plan layout is shown in Fig. 6. The steel columns and beams are box shape and H shape made of Q345 and Q235 steel, respectively. The dead load is 6.0kN/m<sup>2</sup> and the live load is 2.5kN/m<sup>2</sup> for each floor. The structural member sections are listed in Table 2 (Berman 2011). The finite element model of the first story is shown in Fig. 7.

The Tianjin, El Centro, and Loma Prieta earthquake records listed in Table 3 are used as the excitations. Five PGA levels of 0.3g, 0.5g, 0.7g, 1.0g and 1.2g are considered, and the damage indices (*DI*) of the steel frame and internal energy (*E*) of the structure are normalized to the reference story, together with the importance coefficients (*IC*), the optimal maximum control force (*F*) of MR dampers at each story are listed in Table 4. MR dampers are located between the columns as labeled in Fig. 6, there are 4 MR dampers in each framework and total 16 MR dampers at each story.

Table 2 SPSW plate thicknesses and member sizes (mm)

Story	SPSW	Frame column	Boundary column	Beam
1	6.93	□400×37.1	□600×55.3	H363×257×22×13
2	6.93	□400×29.6	□600×55.0	H363×257×22×13
3	6.93	□400×25.6	□600×51.8	H363×257×22×13
4	6.56	□400×25.3	□600×41.4	H363×257×22×13
5	6.48	□400×24.5	□600×40.5	H363×257×22×13
6	6.48	□350×24.5	□500×40.5	H363×257×22×13
7	6.33	□350×23.7	□500×37.4	H363×257×22×13
8	4.85	□350×23.7	□500×37.4	H363×257×22×13
9	4.72	□350×20.0	□500×37.4	H363×257×22×13
10	4.39	□350×18.6	□500×37.4	H363×257×22×13
11	3.66	□300×17.4	□400×37.4	H306×204×24×9
12	3.66	□300×14.2	□400×37.4	H306×204×24×9
13	2.70	□300×12.8	□400×30.6	H306×204×24×9
14	1.55	□300×10.5	□400×30.6	H306×204×24×9
15	1.50	□300×10.0	□400×18.2	H546×313×22×14

Table 3 Earthquake excitations

Name	Event	Year	Duration(s)	Station
TJ	Tianjin	1976	12	Tianjin Hospital
El	El Centro	1940	30	Imperial Valley Irrigation District substation
LP	Loma Prieta	1989	24	APEEL 2-Redwood City

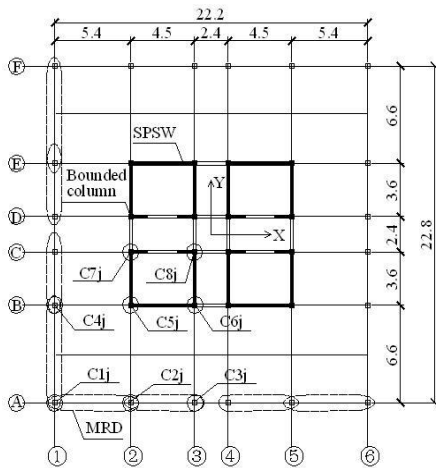


Fig. 6 Plan view of structure

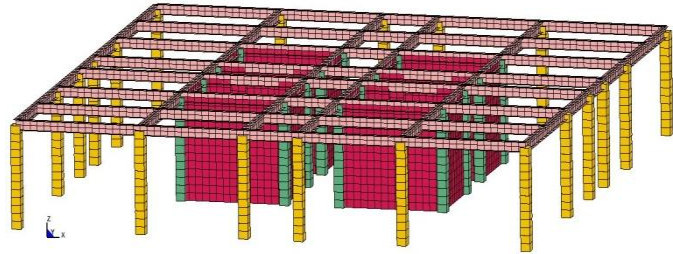


Fig. 7 Finite element model of the first story

Table 4 Maximum control force of MR damper at each story (kN)

Story	1	2	3	4	5	6	7	8	9	10	11	12	13	14	15
<i>E</i>	0.74	1.00	0.85	0.61	0.46	0.63	0.48	0.63	0.57	0.38	0.36	1.00	1.00	1.00	0.31
<i>IC</i>	0.10	0.10	0.10	0.09	0.09	0.09	0.07	0.07	0.07	0.06	0.05	0.05	0.04	0.02	0.01
<i>DI</i>	0.99	1.00	0.97	0.65	0.39	0.68	0.43	0.50	0.60	0.38	0.33	1.00	0.90	1.00	0.00
<i>F</i>	940	871	719	324	143	346	163	193	203	80	56	460	306	195	60

### 5.3 Dynamic responses

A performance comparison between the nonlinear semi-active control strategy and passive-off (zero voltage) and passive-on (maximum voltage) method is shown in Fig.8, which shows the relative displacement time history of 12th story due to PGA of 1.0g Tianjin earthquake. It can be observed that the nonlinear semi-active control system with MR dampers are more effective than the passive methods in reducing structural responses subjected to earthquakes.

The dynamic responses of the preliminary structure (uncontrol), and structure with optimal designed force of MR dampers (nonlinear control) are analyzed due to the PGA of 0.5g, 0.7g, 1.0g and 1.2g Loma Prieta, El Centro and Tianjin earthquakes. The relative displacement envelop curves of different structures in X and Y direction due to Loma Prieta earthquake are shown in Fig. 9, it is indicated that the relative displacements of structures with optimal designed MR dampers are largely reduced, but because the serious weak links exist at the 12th story in X direction and the 12th, 13th and 14th stories in Y direction of the preliminary structure, the deformation concentration phenomena occur and increase with the intensities of earthquakes. For the structure with optimal designed MR dampers, the deformation is more uniform than that of the uncontrolled one, and the control force is more efficiently utilized.

The relative displacement time histories of the 12th story due to Loma Prieta earthquake are shown in Fig. 10 and 11. It is indicated that the residual displacements occur at the 12th story in X direction of the preliminary structure due to the PAG of 0.5g Loma Prieta earthquake, which increase with the intensities of earthquakes and reach nearly 0.2m under the PGA of 1.2g Loma

Prieta earthquake, but the residual displacements are largely reduced by the controlled structures. From the displacement time histories of two structures, it is indicated that the peak responses have been largely reduced by MR dampers, and the oscillation phenomena are decreased during the whole time.

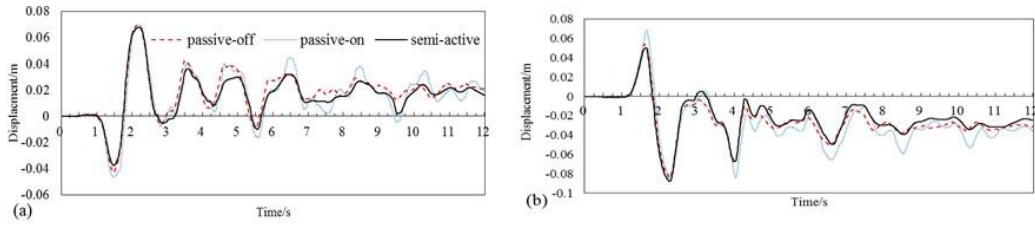


Fig.8 Relative displacement time history of the 12th story in (a) X and (b) Y direction of passive and semi-active control system due to PGA of 1.0g Tianjin earthquake

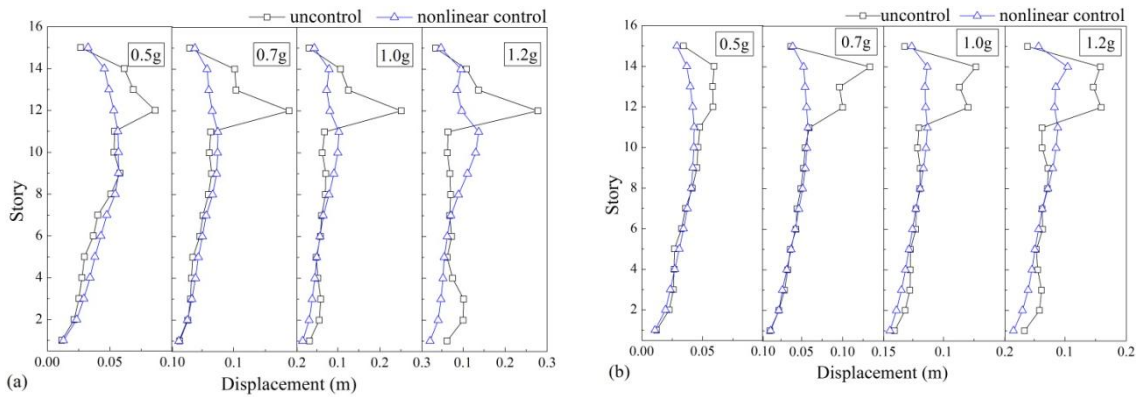


Fig. 9 Relative displacement envelope curves in (a) X and (b) Y direction due to Loma Prieta earthquake

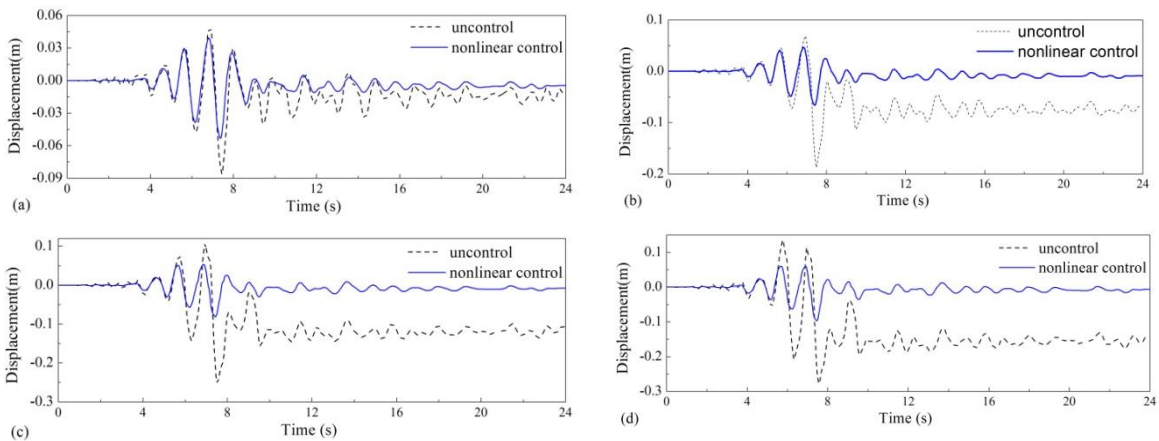


Fig. 10 Relative displacement time histories in X direction of the 12th story due to PGA of (a) 0.5g, (b) 0.7g, (c) 1.0g and (d) 1.2g Loma Prieta earthquake

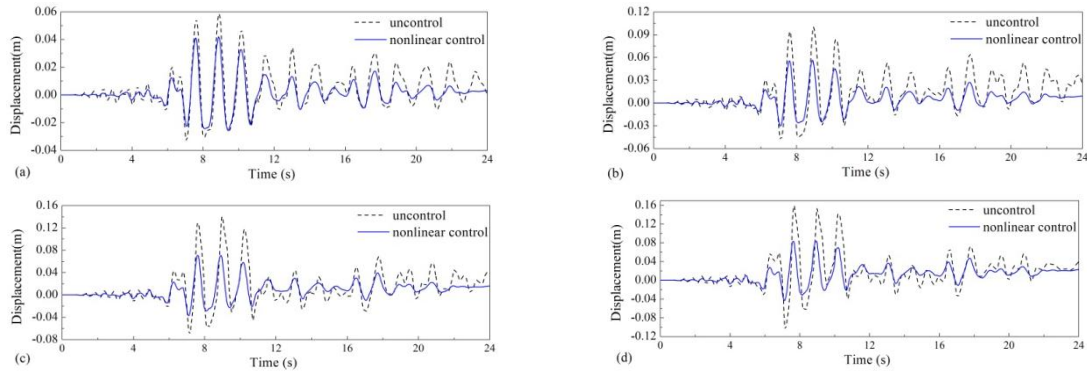


Fig. 11 Relative displacement time histories in Y direction of the 12th story due to PGA of (a) 0.5g, (b) 0.7g, (c) 1.0g and (d) 1.2g Loma Prieta earthquake

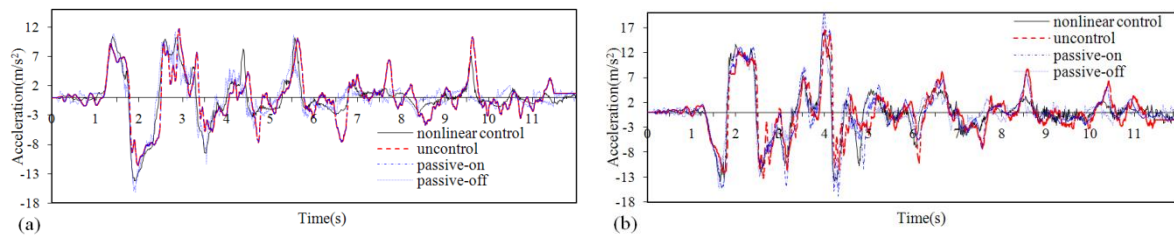


Fig.12 Acceleration time histories in (a) X and (b) Y direction of the roof story due to PGA of 1.0g Tianjin earthquake

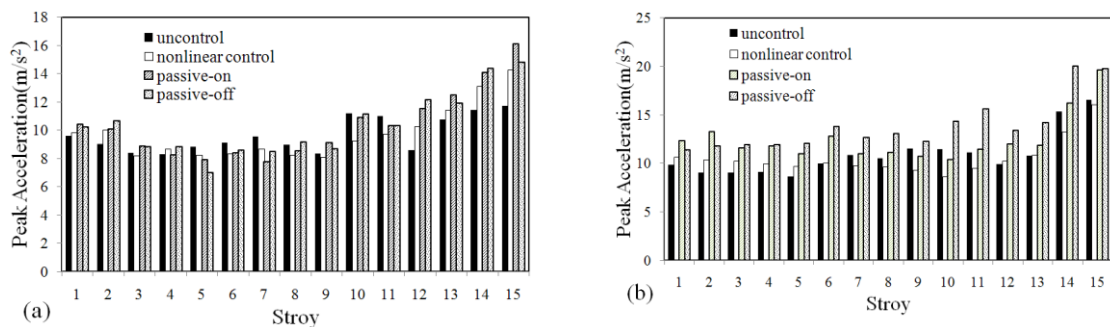


Fig.13 Peak acceleration of each story in (a) X and (b) Y direction due to 1.0g Tianjin earthquake

The acceleration responses at the top floor of the preliminary structure, the nonlinear semi-active controlled structure, and the passive-on and passive-off controlled structures due to PGA of 1.0g Tianjin earthquake are shown in Fig.12 and the peak acceleration values of each story are shown in Fig. 13. It is shown that the acceleration responses of uncontrolled structures have a little increase in some stories because the sample bang-bang control law is used in this control platform and MR dampers are simulated by the virtual beam elements and installed between the beams and columns of structure like bracing members, and the stiffness of preliminary structure has been increased. Comparison with the passive control systems indicate that the acceleration responses of both two passive controlled structures are larger than that of the nonlinear semi-active controlled structure, and the nonlinear semi-active control system has a better performance, as shown in Fig. 13.

### 5.4 Damage analysis

The steel frame columns and the boundary columns of SPSW are classified into 8 categories as shown in Fig. 6, the global damage process of different structures due to the PGA of 0.5g, 0.7g, 1.0g and 1.2g Loma Prieta earthquakes are shown in Fig. 14 and 15, respectively. It is indicated that the damage drifts at the peak acceleration point and increases very slowly at the other times, and the boundary columns have larger damage than that of the steel frame columns at the same story, and the damage of structure with MR dampers is much smaller than that of the uncontrolled one. The global damage of the preliminary structure is controlled by the 12th story, while that of the controlled structures is controlled by the 3rd story due to PGA of 0.5g and 0.7g Loma Prieta earthquakes, which indicates that the MR dampers can strengthen the weak links, such as weak stories or weak position or weak components of structure, and redistribute the seismic performance of structure.

The IDA curves of the global damage indices of the preliminary structure, and structure with optimal designed MR dampers due to the increasing PGA of Loma Prieta, Tianjin and El Centro earthquakes are shown in Fig. 16, and the damage distribution at the odd stories of the steel frame is shown in Fig. 17. From Fig. 16, it is indicated that the control effectiveness of global damage increases with the earthquake intensities, and the structures are more damageable under Loma Prieta earthquakes. From the tendency of the IDA curves, it is obvious to find two turning points at

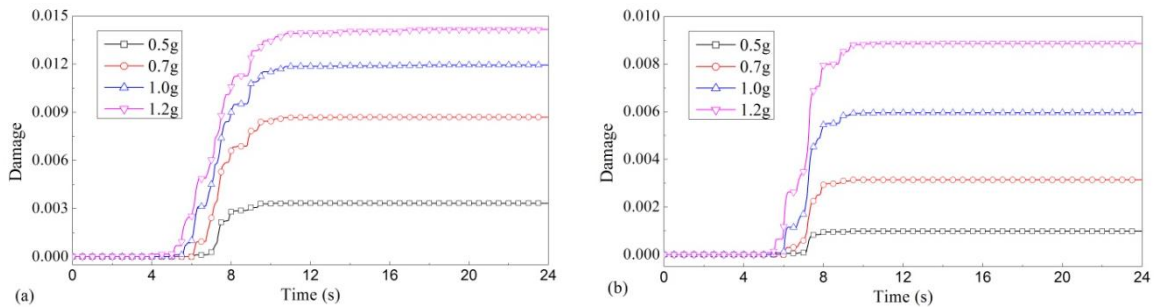


Fig. 14 Damage process of the steel frame due to Loma Prieta earthquake for (a) preliminary structure, and (b) structure with optimal deigned MR dampers

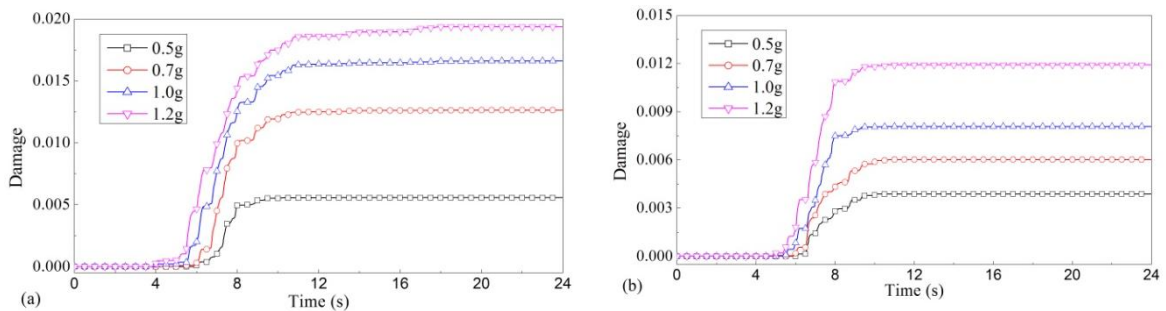


Fig. 15 Damage process of the boundary columns due to Loma Prieta earthquake for (a) preliminary structure, and (b) structure with optimal deigned MR dampers

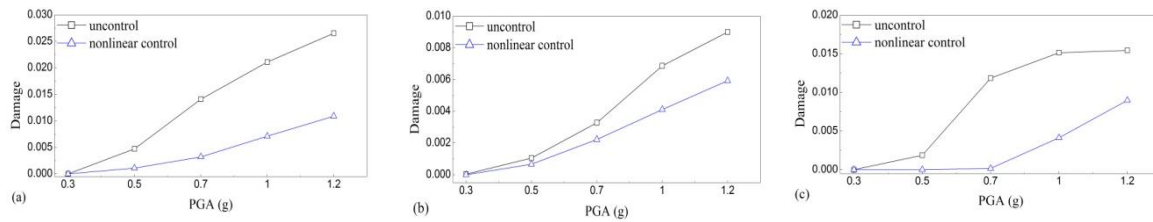


Fig. 16 Global damage of steel frame due to the increasing PGA of (a) Loma Prieta, (b) Tianjin, and (c) El Centro earthquakes

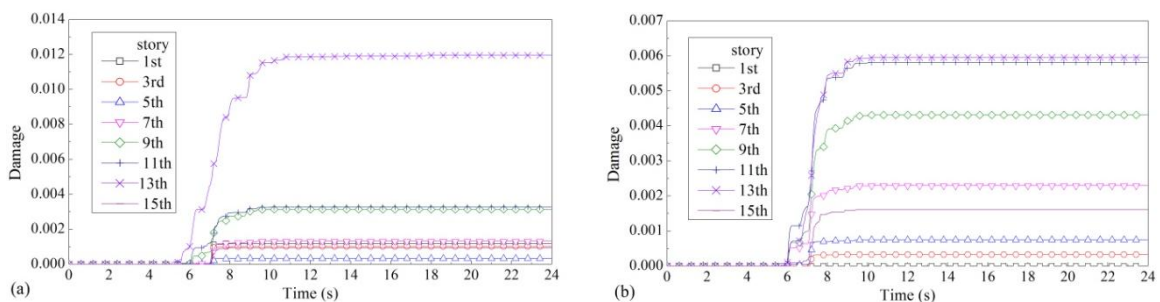


Fig. 17 Damage distribution of steel frame due to 1.0g Loma Prieta earthquake for (a) preliminary structure, and (b) structure with optimal designed MR dampers

the PGA of 0.5g and 0.7g, respectively, the first one is formed because the structure steps into nonlinear response stage, and the second one reflects that the seismic performance of the SPSWs structure has been increased under strong earthquakes, the reason is that more obvious tension strips of the SPSWs are aroused by the strong earthquakes, which will balance parts of the bending moments produced by the shear force and increase the stiffness and strength of structure, therefore, the global seismic performance has been increased. From Fig. 17, it is indicated that the damage trend is similar for different stories, i.e. the damage drifts at the peak point of acceleration, and is stable at other times. The damage of controlled structure is much smaller than that of uncontrolled one, and the damage of the preliminary structure is concentrated on the 11th story (the 12th story is not depicted in this figure), while the controlled structures have a much wider damage distribution.

## 6. Conclusions

A semi-active control platform comprising the Bouc-Wen model of MR damper, the simple bang-bang semi-active control law, and the steel damage material model is developed in LS-DYNA program. During the simulation, the main structure is simulated by the general finite element program and each MR damper is simulated by a virtual beam element, based on the data transferring between the main program and the control platform, it can realize the purpose of integrated modeling, analysis and design of the nonlinear semi-active control system. The numerical simulation method of SPSW, the damage criteria of steel frame and the optimal designed control force of MR dampers at each story are also proposed. The seismic control

effectiveness is verified by the numerical example of a 15-story steel frame-SPSW structure, which indicates that the control platform and the numerical method are stable and fast, the relative displacement, shear force, and damage of the structure are largely reduced using optimal designed MR dampers, and the formation of tension strips of SPSWs is also delayed and mitigated significantly. However, because of the limit capacity of MR dampers, the control effectiveness decreases after a certain intensity of earthquake actions, and the residual displacement cannot be eliminated completely as well.

### Acknowledgements

The writers gratefully acknowledge the partial support of this research by the National Natural Science Foundation of China under Grant No. 51322806, the Fundamental Research Funds for the Central Universities under Grant No. 2014JBZ011, and the National Basic Research Program of China (973 Program) under Grant No. 2011CB013603 and 2011CB013606.

### References

- Berman, J.W. (2011), "Seismic behavior of code designed steel plate shear walls", *Eng. Struct.*, **33**(1), 230-244.
- Bonora, N. (1997), "A nonlinear CDM model for ductile failure", *Eng. Fract. Mech.*, **58**, 11-28.
- Dyke, S.J., Spencer Jr., B.F. (1996), "Seismic response control using multiple MR dampers", *Proceedings of the 2nd International Workshop on Structure Control*, pp. 163-173, Hong Kong.
- Feng, Q. and Shinozuka, M. (1990), "Use of a variable damper for hybrid control of bridge response under earthquake", *Proceedings of the US National Workshop on Structure Control Research*, USC Publication No. CE-9013, pp. 107-112, Los Angeles, CA, USA.
- Foutch, D.A. and Yun, S.Y. (2002), "Modeling of steel moment frames for seismic loads", *J. Constr. Steel Res.*, **58**(5-8), 529-564.
- Jansen, L.M. and Dyke, S.J. (2000), "Semiactive control strategies for MR dampers: comparative study", *J. Eng. Mech.-ASCE*, 2000, **126**(8), 795-803.
- Johnson, E.A. and Erkus, B. (2007), "Dissipativity and performance analysis of smart dampers via LMI synthesis", *Struct. Control Hlth.*, **14**(3), 471-496.
- Kim, Y., Langari, R. and Hurlebaus, S. (2008), "Semiactive nonlinear control of a building with magnetorheological damper system", *Mech. Syst. Signal Pr.*, **23**(2), 300-315.
- Lee, D.Y. and Wereley, N.M. (2000), "Analysis of electro-and magnetorheological flow mode dampers using Herschel-Bulkley model", *Processing of the SPIE, Smart Structures and Materials: Damping and Isolation*, pp. 244-255, Newport Beach, CA, USA, March 6.
- Li, L., Song, G. and Ou, J.P. (2010), "A genetic algorithm-based two-phase design for optimal placement of semi-active dampers for nonlinear benchmark structure", *J. Vib. Control*, **16**(9), 1379-1392.
- Li, Q.S., Liu, D.K., Leung, A.Y.T., Zhang, N., Luo, Q.Z. (2002), "A multilevel genetic algorithm for optimum design of structural control systems", *Int. J. Numer. Meth. Eng.*, **55**(7), 817-834.
- Lin, W., Li, Z.X. and Ding, Y. (2008), "Trust-region based instantaneous optimal semi-active control of long-span spatially extended structures with MRF-04K damper", *Earthq. Eng. Vib.*, **7**(4), 447-464.
- Liu, X., Begg, D.W., Mattravers, D.R. (1997), "Optimal topology/actuator placement design of structures using SA", *J. Aerospace Eng.-ASCE*, **10**(3), 119-125.
- Lu, Q., Peng, Z., Chu, F., Huang, J. (2003), "Design of fuzzy controller for smart structures using genetic

- algorithms”, *Smart Mater. Struct.*, **12**(6), 979-986.
- Ohtori, Y., Spencer, B.F., Jr. and Dyke, S.J. (2004), “Benchmark control problems for seismically excited nonlinear buildings”, *J. Eng. Mech.-ASCE*, **130**(4), 366-385.
- Pirondi, A., Bonora, N., Steglich, D., et al. (2006), “Simulation of failure under cyclic plastic loading by damage models”, *Int. J. Plasticity*, **22** (11), 2146-2170.
- Salawu, O.S. (1997), “Detection of structural damage through changes in frequency: a review”, *Eng. Struct.*, **19**(9), 718-723.
- Thorburn, L.J., Kulak, G.L., Montgomery, C.J. (1983), “Analysis of steel plate shear walls”, Structural Engineering Report No. 107, University of Alberta, Edmonton, Alberta.
- Wang, D.H. and Liao, W.H. (2005), “Modeling and control of magnetorheological fluid dampers using neural networks”, *Smart Mater. Struct.*, **14**(1), 111-126.
- Wongprasert, N., Symans, M.D. (2004), “Application of a genetic algorithm for optimal damper distribution within the nonlinear seismic benchmark building”, *J. Eng. Mech.-ASCE*, **130**(4), 401-406.
- Xu, L.H. and Li, Z.X. (2008), “Semiactive multi-step predictive control of structures using MR dampers”, *Earthq. Eng. Struct. D.*, **37**(12), 1435-1448.
- Xu, L.H. and Li, Z.X. (2011), “Model predictive control strategies for protection of structures during earthquakes”, *Struct. Eng. Mech.*, **40**(2), 233-243.
- Yoshida, O. and Dyke, S.J. (2004), “Seismic control of a nonlinear benchmark building using smart dampers”, *J. Eng. Mech.-ASCE*, **130**(4), 386-392.